Phase transitions in Cd_3P_2 at high pressures and high temperatures

F.S. Yel'kin [a], V.A. Sidorov [a], A. Waśkowska [b], L. Gerward [c,*],
J. Staun Olsen [d], G. Vaitheeswaran [e,1], V. Kanchana [e,1]

[a] *Institute for High Pressure Physics, Russian Academy of Sciences, 142190 Troitsk, Moscow Region, Russia*
[b] *Institute of Low Temperature and Structure Research, Polish Academy of Sciences, 50422 Wroclaw, Poland*
[c] *Department of Physics, Technical University of Denmark, 2800 Lyngby, Denmark*
[d] *Niels Bohr Institute, Oersted Laboratory, University of Copenhagen, 2100 Copenhagen, Denmark*
[e] *Max-Planck-Institut für Festkörperforschung, Heisenbergstrasse 1, 70569 Stuttgart, Germany*

Abstract

The high-pressure, high-temperature structural behaviour of Cd_3P_2 has been studied using electrical resistance measurements, differential thermal analysis, thermo baric analysis and X-ray diffraction. At room temperature, a phase transformation is observed at 4.0 GPa in compression. The experimental zero-pressure bulk modulus of the low-pressure phase is 64.7(7) GPa, which agrees quite well with the calculated value of 66.3 GPa using the tight-binding linear muffin-tin orbital method within the local density approximation. Tentatively, the high-pressure phase has an orthorhombic crystal structure with space group *Pmmn* (#59). The relative volume change at the phase transition is $\Delta V/V = -5.5\%$. Amorphization of the sample occurs above 25 GPa. A *P–T* phase diagram of Cd_3P_2 has been constructed. A metastable phase is observed at ambient conditions after heating the sample to above 600 K at about 3 GPa. A hexagonal unit cell can describe the crystal structure of the metastable phase.
© 2006 Elsevier B.V. All rights reserved.

1. Introduction

The crystal structure of Cd_3P_2 at ambient conditions was first determined by Stackelberg and Paulus [1] and later re-determined by Pistorius et al. [2]. The latter authors also measured the melting curve of Cd_3P_2 in the pressure range 0–4 GPa. Haacke and Castellion [3], and Zdanowicz and Wojakowski [4] have described the preparation of Cd_3P_2 and its semiconducting properties. Experimental studies have been reported on various properties, such as thermoelectric power and the optical gap [3], transport properties [4], photoluminescence and optically pumped laser action [5–7], and energy band structure and other optical properties [8]. Cisowski et al. [9] measured the electrical resistivity and the Hall coefficient as functions of pressure up to 1.2 GPa. Rao and Nayak [10] have prepared Zn_3P_2–Cd_3P_2 solid solutions and measured the lattice parameters and the electrical conductivity. However, little is known about the compressibility and crystal structure stability of Cd_3P_2, and about possible phase transformations at high pressures and high temperatures.

First energy band calculations for Cd_3P_2 were performed by Lin-Chung [11], using a theoretical pseudo potential method in the hypothetical crystal structure, in which the conduction band effective masses as well as the inter band transition assignments, associated with the optical reflectivity peaks, were deduced. Plenkiewicz and Dowgiallo-Plenkiewicz [12,13] have carried out further studies on the band structure and symmetry operations of Cd_3P_2 in the real-crystal symmetry. They used a pseudo potential method, in which a qualitative explanation of the band structure and the optical properties could be made.

Band structure calculations of Cd_3P_2 for its real symmetry encounter many difficulties, and apparently some approximations are necessary. The main reason for these difficulties is the

---

complicated crystal structure. Cd_3P_2 crystallizes in a primitive tetragonal lattice with eight molecules or 40 atoms per unit cell. Hence, only a few theoretical calculations are reported in the literature.

The present work is an experimental and theoretical study of the equation of state of Cd_3P_2 and of phase transformations at high pressures and high temperatures. Some preliminary room temperature results of this study were reported at the Joint 20th AIRAPT–43rd EHPRG Conference [14].

2. Experimental

Electrical resistance measurements and differential thermal analysis (DTA) were performed on single crystals and polycrystalline samples of Cd_3P_2 using a toroid type high-pressure device [15,16]. The device allowed hydrostatic pressures up to 8 GPa and temperatures up to 800 K. A Teflon capsule, containing the sample, a heater and a manganin gauge for pressure measurement, was filled with a suitable pressure-transmitting medium (4:1 methanol:ethanol up to 500 K, and 1:1 pentane:ether up to 800 K). It was then placed in the central hole of a lithographic stone gasket and compressed by two profiled anvils made of a hard tungsten–carbide alloy.

The volume of the Teflon capsule is about one cm^3, and a spacer made of a porous thermal insulation material divides it into two zones. A nickel–chrome heater is situated in the hot zone, containing the sample, whereas the manganin pressure gauge remains near room temperature in the cold zone. The sample temperature is measured by a chromel–alumel thermocouple made of a wire with thickness 50 μm. The pressure inside the Teflon capsule is monitored upon heating and cooling the sample. A volume change due to a phase transition will result in a discontinuous change in the otherwise monotonous pressure–temperature dependence. This method of establishing the transition temperature could appropriately be called thermobaric analysis (TBA). It may be considered the pressure analogue of the well-known method of differential thermal analysis (DTA).

Electrical measurements were performed on needle-like single crystals with typical dimensions 0.3 mm × 0.3 mm × 1.5 mm. Four contacts were soldered to the sample with the use of tin. Thus, the electrical resistance measurements were limited to temperatures below the melting point of tin at about 505 K. DTA and TBA were performed on 0.7 mm × 0.7 mm × 2 mm samples at temperatures up to about 800 K. Khvostantsev et al. [17] have described the experimental techniques in more detail.

Room temperature, high-pressure powder X-ray diffraction (XRD) patterns were recorded at HASYLAB-DESY in Hamburg, Germany, using the white-beam method and synchrotron radiation. Olsen [18] has described the diffractometer, working in the energy-dispersive mode. High pressures were obtained in a Syassen–Holzapfel type diamond-anvil cell [19]. A finely ground powder sample and a ruby chip as a pressure marker were placed in a hole with diameter 200 μm in an Inconel gasket, pre-indented to a thickness of 60 μm. A 16:3:1 methanol:ethanol:water mixture was used as the pressure-transmitting medium. The pressure was determined by the ruby luminescence method, applying the non-linear pressure scale of Mao et al. [20]. The Bragg angle of each run was calculated from a zero-pressure spectrum of sodium chloride (NaCl) in the diamond-anvil cell.

XRD spectra were recorded at pressures up to 30 GPa. At each pressure, values for the lattice parameter and the unit cell volume were derived and refined using the PURUM code [21]. The compression curve can then be described by the Birch–Murnaghan equation of state [22,23]:

$$P = \frac{3}{2} B_0 (x^{-7/3} - x^{-5/3}) \left[1 - \frac{3}{4}(4 - B_0')(x^{-2/3} - 1) \right] \tag{1}$$

where $x = V/V_0$, V being the volume at pressure P, and V_0 the volume at zero-pressure, B_0 is the bulk modulus and B_0' is the pressure derivative, both parameters evaluated at zero-pressure. Numerical values of B_0 and B_0' were obtained from a non-linear least-squares fit of Eq. (1) to the experimental pressure–volume data points.

3. Theoretical procedure

In the present work, we have used a tight-binding linear muffin-tin orbital method [24] within the local density approximation [25] to calculate the total energies and ground state properties. The atomic sphere approximation (ASA) has been used [26]. In this method the crystal is divided into space filling spheres centred on each atomic site. Empty spheres were introduced in the high symmetry interstitial sites. Combined correction terms are also included, which account for the non-spherical shape of the atomic sphere and the truncation of higher partial waves inside the spheres to minimize the errors in the LMTO method.

The positions and the radii of the interstitial spheres were calculated using an automated procedure developed by Krier et al. [27]. The scalar relativistic Kohn–Sham–Schrödinger equations were solved taking all relativistic effects into account except for the spin-orbit coupling. The experimental atomic positions were used in the present work to calculate the total energies. In order to calculate the total ground state properties, total energies were calculated for several volumes. The Birch–Murnaghan equation (1) was then fitted to the calculated pressure–volume data to yield the bulk modulus and its pressure derivative.

4. Results and discussion

At ambient conditions, Cd_3P_2 crystallizes in a structure of the Zn_3P_2 type. It can be described in the tetragonal system, space group $P4_2/nmc$ (137) with a unit cell of dimensions $a_0 = 8.7537$ Å and $c_0 = 12.2669$ Å [2]. The unit cell contains eight formula units, giving a molar volume $V_m = 117.5$ Å^3 per molecule. The Cd atoms, coordinated by the P atoms, are situated in three of four deformed tetrahedral sites, whereas the P atoms are surrounded by the Cd atoms, located at six of eight corners of the cube. Two diagonally opposite corners of the cube remain vacant (cf. Fig. 1). It should be noted that a larger unit cell containing 16 molecules would be nearly cubic, since c_0 is almost equal $a_0\sqrt{2}$.

4.1. Room temperature compression of Cd_3P_2

Fig. 2 shows that the electrical resistance of Cd_3P_2 increases linearly with pressure up to 4.0 GPa. At this pressure the resistance increases sharply by about 15 times, indicating a phase transition. Upon further increase of pressure, the resistance continues to rise and passes through a shallow maximum at about 7 GPa. In decompression, the resistance exhibits a sudden jump at 2.4 GPa indicating the reverse transition and a hysteresis of 1.6 GPa. At the reverse transition, the resistance increases, though one may expect it to decrease. Moreover, the slope dR/dP for the low-pressure phase is much larger in decompression than initially observed in compression. However, XRD shows that the initial tetragonal structure is retained at ambient pressure.

The above observations may be explained by a redistribution of defects at the phase transitions in compression and decompression, taking into account that Cd_3P_2 is a self-doped semiconductor. Therefore, the electrical properties in compres-
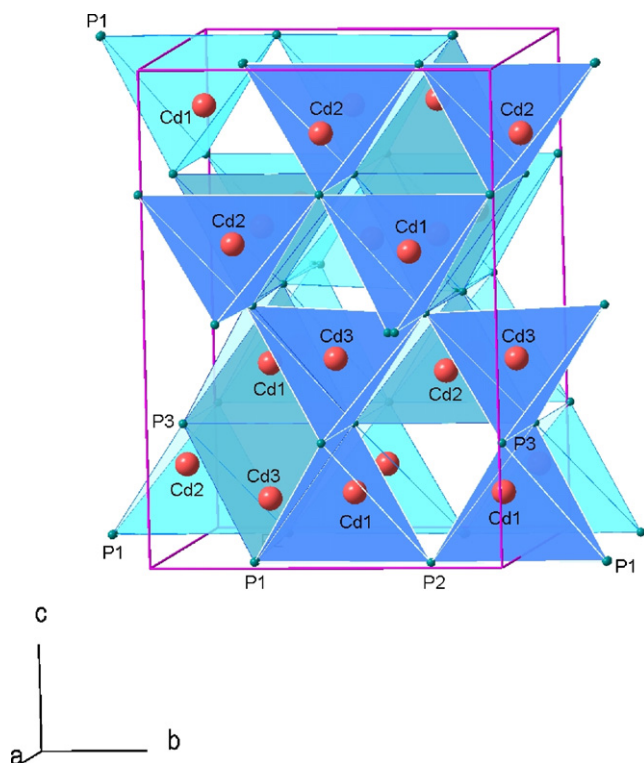
Fig. 1. Crystal structure of Cd_3P_2 in the tetragonal phase, space group $P4_2/nmc$ (137).

Fig. 3. X-ray diffraction spectra of Cd_3P_2, recorded at various pressures, using synchrotron radiation. The Bragg angle is $\theta = 4.955°$. Note the phase transformation at 4.0 GPa and complete amorphization at 28 GPa. The strong peaks at 23.11 and 26.09 keV are Cd Kα and Kβ fluorescence lines.

sion and decompression may be different. Moreover, a single crystal transforms to a polycrystalline sample at the phase transition. This was confirmed by experiments, where the same sample was cycled through the region of the phase transitions a few times. In fact, the slope dR/dP and the value of the resistance of the low-pressure phase return to their initial values after the second cycle.

Fig. 3 shows a series of synchrotron X-ray diffraction (XRD) spectra for Cd_3P_2 recorded at various pressures. The XRD spectra clearly indicate a pressure-induced structural phase
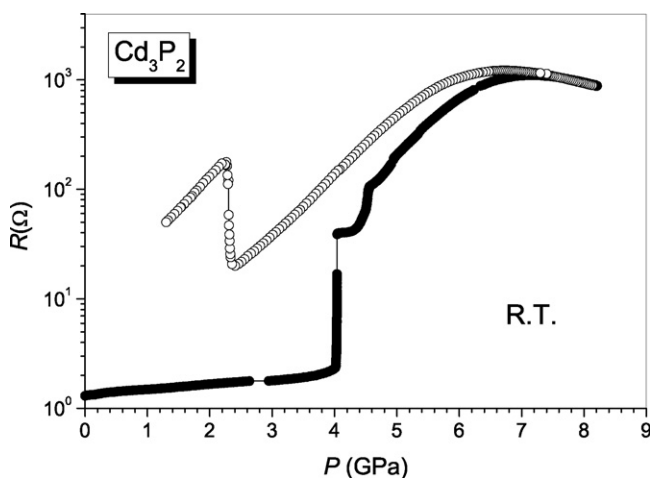

Fig. 2. Pressure dependence of the electrical resistance of a Cd_3P_2 sample at room temperature. Filled circles denote compression, and open circles decompression. Note the phase transformation at 4.0 GPa upon compression and the hysteresis in decompression.
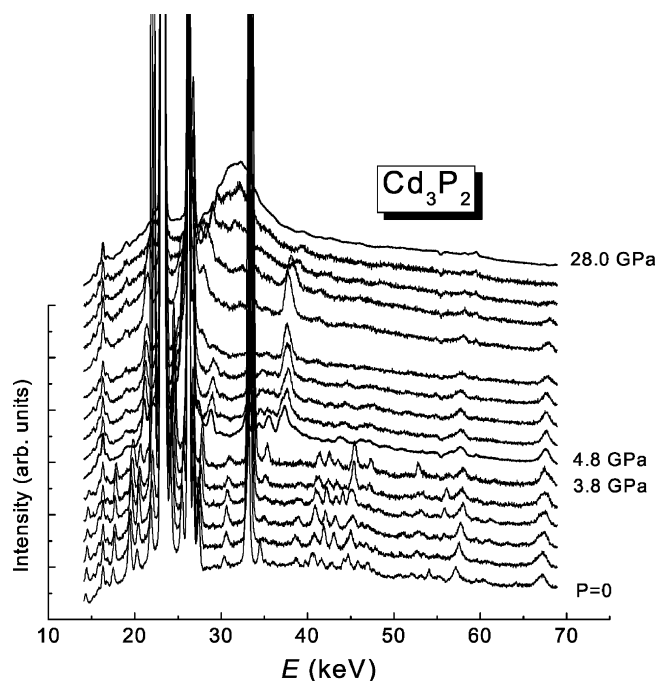
transformation at about 4 GPa. Thus, the transition pressure of 4.0 GPa, found by the resistance measurement and described above, is distinctively confirmed. At much higher pressures, the growing continuous background in the XRD spectra indicates an amorphization of Cd_3P_2. As seen in Fig. 3, the sample is completely amorphous at 28 GPa, where the XRD spectrum consists of a single broad peak with a maximum at 32.3 keV. This value corresponds to a nearest-neighbour distance of 2.2 Å between the Cd_3P_2 molecules.

Fig. 4 shows the compression of tetragonal Cd_3P_2 at room temperature. A fit of the Birch–Murnaghan equation (1) to the experimental pressure–volume data points gives the zero-pressure bulk modulus $B_0 = 64.7(9)$ GPa and the pressure derivative $B'_0 = 4.3(7)$. It should be noted that it is difficult to measure the curvature of the compression curve in the small pressure range 0–4 GPa, hence the large uncertainty in B'_0. The low value of the bulk modulus indicates that Cd_3P_2 is highly compressible, i.e. a soft material. To the best knowledge of the authors, there are no published data with which to compare the present results.

The compression curve calculated by the LMTO–ASA method is shown by the full curve in Fig. 4. The theoretical bulk modulus is $B_0 = 66.3$ GPa, which is 2.5% larger the experimental value given above. For the pressure derivative, the calculations give $B'_0 = 5.11$. At zero-pressure, the predicted lattice parameters are $a_0 = 8.8182$ Å and $c_0 = 12.3570$ Å, giving a molar volume $V_m = 120.11$ Å^3 per molecule. The latter value is 2% larger than the corresponding experimental value (cf. Fig. 4).

As pointed out by Pistorius et al. [2], it is likely that the high-pressure phase of Cd_3P_2 is structurally related to $Cd_3As_2^V$ and
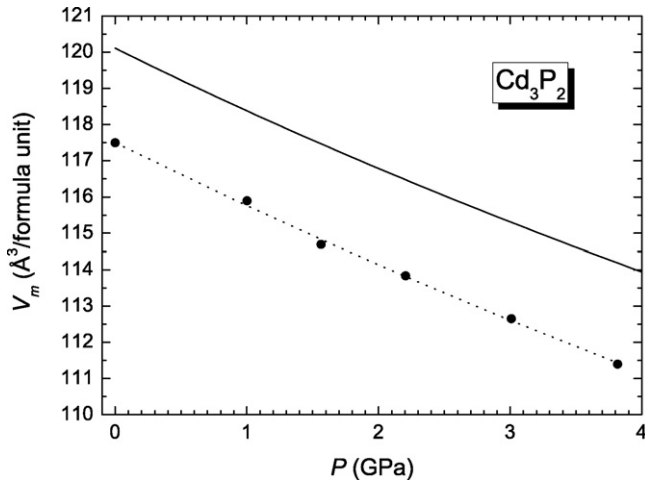
Fig. 4. Compression of tetragonal Cd_3P_2 at room temperature. The dashed curve through the experimental data points has been calculated from the Birch–Murnaghan equation (1). The result of the theoretical calculation is shown by the full curve.

Zn_3As_2[V]. The crystal structure of the latter phases, in turn, is probably the same as the one found in Cd_3Sb_2 and Zn_3Sb_2 at ambient conditions, as suggested by Pistorius [28]. The space group is *Pmmn* (59), and the orthorhombic unit cell contains six formula units. The crystal structure of Cd_3Sb_2 and Zn_3Sb_2 has been reported by Dobryden [29] and by Psarev and Dobryden [30], respectively.

Our XRD data for pressures above 4.0 GPa are indeed consistent with the hypothesis that the unit cell of the Cd_3P_2 high-pressure phase is orthorhombic with space group *Pmmn* (59). At 4.82 GPa the unit cell parameters are $a = 7.55(15)$ Å, $b = 6.96(15)$ Å, and $c = 11.03(20)$ Å. The *d*-spacing of the low- and high-pressure phases as functions of pressure is shown in Fig. 5. The experimental compression curves of tetragonal and orthorhombic Cd_3P_2 are plotted in Fig. 6. It is seen that there is a volume collapse at the phase transition. The relative
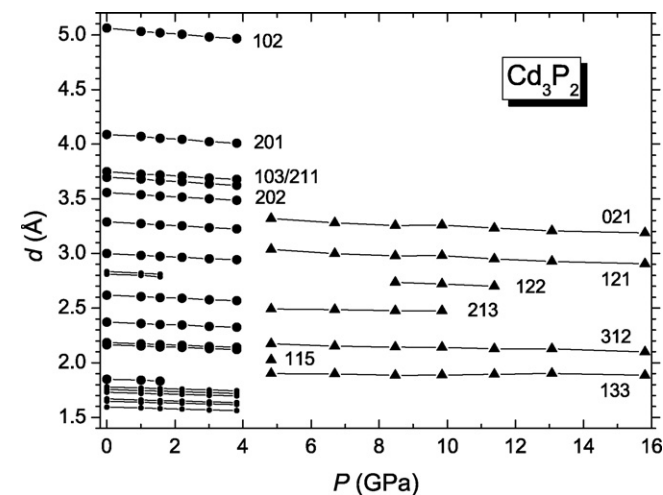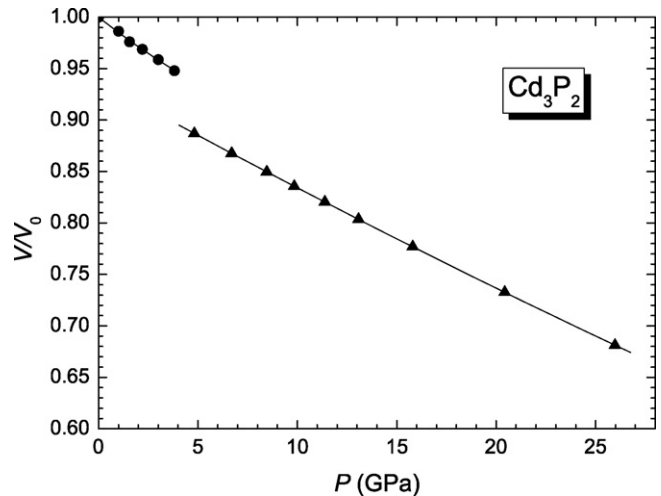

Fig. 6. Experimental compression curves of Cd_3P_2. The notation is as in Fig. 5. The relative volume change at the tetragonal to orthorhombic transition is $\Delta V/V = -5.5\%$.

volume change at the tetragonal-to-orthorhombic transition is $\Delta V/V = -5.5\%$.

4.2. The phase diagram of Cd_3P_2

The transition, found at room temperature at 4.0 GPa, can be observed up to 500 K in the isothermal cycle of pressure change as shown in Fig. 7. At 500 K the transition pressure is 3.6 GPa. The hysteresis loop between the transition in compression and decompression is 0.9 GPa, which is less than 1.6 GPa observed at room temperature.

The initial tetragonal phase is a semiconductor, and the resistivity depends strongly on temperature and pressure. For a given pressure, the resistivity decreases with increasing temperature. The high-pressure orthorhombic phase is metal-like, and its resistivity increases with increasing temperature. In the pressure range 2.4–2.6 GPa, where the reverse transition takes place, the tetragonal phase has a much stronger temperature dependence of resistivity than the orthorhombic phase. Therefore, at the reverse

Fig. 5. The observed lattice plane spacing, *d*, are shown as a function of pressure. Filled circles denote the tetragonal phase, and filled triangles the orthorhombic phase. For clarity, indices *h k l* are shown only for the first five lines of the tetragonal phase. The full lines are guides for the eye.
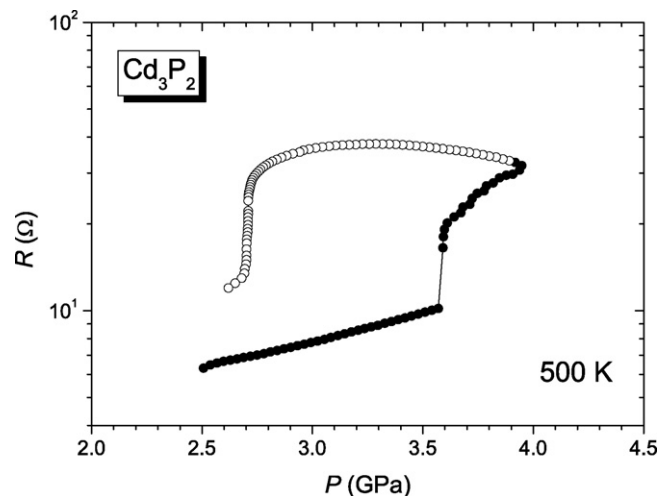

Fig. 7. Pressure dependence of the electrical resistance of a Cd_3P_2 sample at 500 K. The notation is as in Fig. 2.

transition, the sample exhibits a *rise* in resistance at ambient temperature (Fig. 2), and a *drop* at 500 K (Fig. 7). Actually, there would be no change at about 420 K according to our measurement of the resistance as a function of temperature for the two phases.

Unfortunately, the resistance measurements could not be extended to temperatures above 500 K, since the tin solder would melt. However, two DTA and TBA experiments were performed above 600 K.

No phase transitions was observed when a single crystal was heated at $P = 3.5$ GPa from room temperature to 733 K at a rate of 3 K/s. The temperature was then returned to room temperature, the pressure was decreased to 2.7 GPa, and another heating experiment was performed. The DTA and TBA signals showed the presence of an irreversible phase transition at pressure 2.9 GPa, and temperature 675–690 K (Fig. 8a and b). The temperature interval, which roughly corresponds to the size of the open triangle in Fig. 9, is due to the high heating rate and the kinetics of the transition.

The above experiments were repeated using a powdered polycrystalline sample as the starting material. The TBA anomaly,
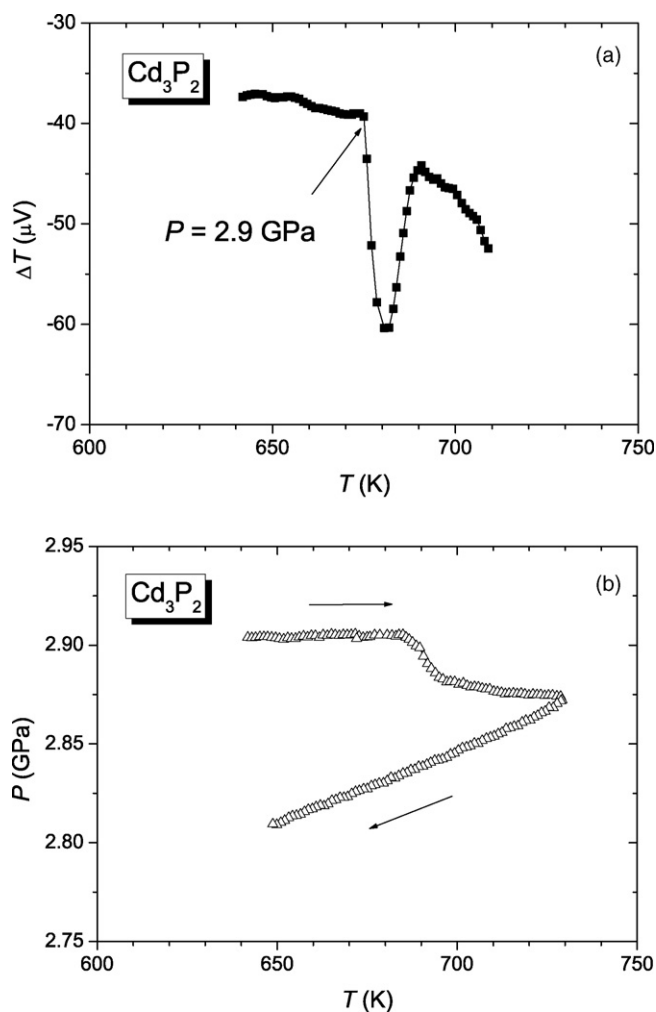

Fig. 9. *P–T* diagram of phase transitions in Cd_3P_2, observed by resistance measurements. Solid symbols denote compression, and open symbols decompression. Triangles denote regions, where a metastable phase is formed. The solid line is the melting curve of Cd_3P_2 [2].

Table 1

Observed and calculated *d* spacings of the metastable phase at ambient conditions (cf. Fig. 10)

2θ (°)	d_{obs} (Å)	d_{calc} (Å)	Intensity (arbitrary units)	$h\,k\,l$
24.969*	3.5632	3.5612	28	0 0 2
28.944	3.0823	3.0953	13	3 2 0/4 0 1
30.534*	2.9253	2.9277	88	2 1 2
31.965*	2.7975	2.8009	52	3 0 2
34.721*	2.5815	2.5900	21	3 1 2
35.357*	2.5365	2.5419	18	5 0 1
36.788	2.4411	2.4436	9	5 1 0
38.431*	2.3404	2.3388	100	1 0 3
42.353*	2.1323	2.1340	12	4 3 1
43.519*	2.0778	2.0748	34	6 1 0
44.367	2.0401	2.0318	9	2 2 3
46.646*	1.9456	1.9468	17	4 0 3
47.388*	1.9168	1.9127	40	6 0 2
48.130*	1.8890	1.8896	20	3 2 3
50.886	1.7930	1.7927	9	6 1 2
51.257	1.7809	1.7806	7	0 0 4
51.893	1.7605	1.7622	6	1 0 4/3 3 3
53.589	1.7087	1.7061	7	7 0 2
56.822*	1.6189	1.6187	10	7 2 1
57.458	1.6025	1.6052	8	5 2 3
60.532*	1.5283	1.5270	9	4 1 4
61.486*	1.5068	1.5062	16	7 2 2
62.546*	1.4838	1.4845	12	8 2 0
63.500*	1.4638	1.4639	13	4 2 4
65.514	1.4236	1.4245	4	0 0 5
67.263	1.3908	1.3915	5	9 0 2
68.800	1.3634	1.3616	6	7 2 3
72.085*	1.3091	1.3092	19	6 6 0
76.007*	1.2510	1.2513	10	3 3 5
76.908*	1.2386	1.2387	10	9 3 1
80.353*	1.1940	1.1940	11	8 3 3
83.003	1.1624	1.1624	7	9 4 1/7 3 4

Wavelength $\lambda = 1.54056$ Å (Cu Kα_1). Asterisks (*) denote reflections used for the unit cell determination and refinement procedure (see text). Hexagonal unit cell with $a_0 = 15.7102(32)$ Å, $c_0 = 7.1225(25)$ Å, and $V_0 = 1522.4(7)$ Å^3. The uncertainty, given in parenthesis, is the estimated standard error of the fit in units of the last decimal place.

Fig. 8. Signals obtained on heating a single crystal of Cd_3P_2 to 733 K at 2.7–2.9 GPa, indicating the formation of a metastable phase: (a) DTA and (b) TBA.
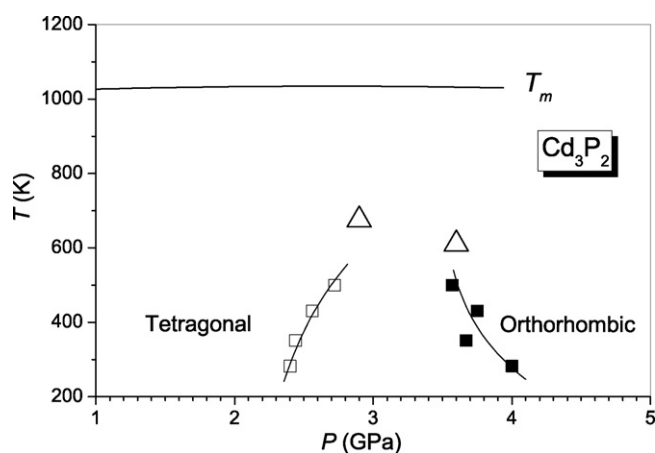
Table 2
Lattice parameters of Cd_3P_2 phases

	a (Å)	b (Å)	c (Å)	Reference
Tetragonal (stable, ambient conditions)	8.7537		12.2669	[2]
Orthorhombic (high-pressure phase at 4.6 GPa)	7.55(10)	6.96(10)	11.03(15)	Present work
Hexagonal (metastable, ambient conditions)	15.7107(32)		7.1225(25)	Present work

similar to the one in Fig. 8b, was observed on heating the powder sample at $P = 3.6$ GPa to $T = 610$ K. No appreciable DTA anomaly was observed. Subsequent heating to 740 K at 2.7 GPa, and to 770 K at 2.5 GPa showed no DTA or TBA anomalies.

A *P–T* phase diagram, constructed on the basis of electrical resistance, DTA and TBA measurements is shown in Fig. 9. The transition pressure in compression is 4.0 GPa at room temperature and decreases at higher temperatures. The hysteresis of the transition also decreases at high temperature. On further increase of temperature above 600 K this simple picture of a reversible first-order phase transition is no longer valid, and the formation of a metastable phase is observed. This will be described in the next section.

4.3. A metastable phase of Cd_3P_2

A metastable phase of Cd_3P_2 has been found in samples heated to above 600 K at about 3 GPa (cf. experimental points denoted by triangles in Fig. 9). Fig. 10 shows the XRD pattern of the metastable phase of Cd_3P_2 at ambient conditions. This particular sample had been heated to 720 K at 3.6 GPa. Repeated XRD measurements after having kept the sample at room temperature for a few months demonstrated the stability of the new phase—no changes were found in the XRD patterns.

The diffraction pattern of the metastable phase has been interpreted and indexed using the PowdMult code [31]. First, 20 major diffraction peaks were successfully indexed, assuming a hexagonal unit cell. Then, the unit cell parameters were refined

Fig. 10. Powder X-ray diffraction spectrum of the metastable phase of Cd_3P_2 at ambient conditions. The wavelength of the X-rays is $\lambda = 1.54056$ Å (Cu Kα_1). The metastable phase was obtained by heating the sample to 720 K at 3.6 GPa. For clarity, indices are shown only for major reflections (cf. Table 1, where all reflections are indexed).

using the least-squares code PURUM [21]. Finally, the observed and calculated *d* spacing was calculated and compared for *all* observed peaks in the diffraction pattern. The result is shown in Table 1. We can argue that the composition of metastable phase is Cd_3P_2, since all peaks in the observed diffraction–pattern have been indexed in hexagonal symmetry. Otherwise some diffraction lines should have been identified as lines of other (known, more simple) phases.

The goodness of the fit can be described by:

$$\frac{\sum |d_{obs} - d_{calc}|}{\sum d_{obs}} = 9.4 \times 10^{-4} \tag{2}$$

which is quite satisfactory.

The resulting parameters of the hexagonal unit cell at ambient conditions are $a_0 = 15.7102(32)$ Å and $c_0 = 7.1225(25)$ Å. This gives a unit cell volume of $V_0 = 1522.4(7)$ Å^3. Assuming the same molar volume as in the original tetragonal phase ($V_m = 117.5$ Å^3 per formula unit), would give 13 formula units in the hexagonal unit cell. However, it is probable that the density of the metastable phase is larger than that of the tetragonal low-pressure phase.

Table 2 summarizes the unit cell dimensions of the Cd_3P_2 phases observed in the present work. It is seen that $a_h \approx \sqrt{a_t^2 + c_t^2}$ and $c_h \approx b_{orth}$. This would mean that after decompression the structural polyhedra in the hexagonal metastable phase have relaxed to the dimensions they had originally in the *ac* plane of the tetragonal phase, whereas the deformation along *b*-axis of the orthorhombic phase is retained.

5. Conclusions

The high-pressure and high-temperature behaviour of Cd_3P_2 has been studied using electrical resistance measurements, differential thermal analysis (DTA), thermo baric analysis (TBA) and X-ray diffraction (XRD). A reversible first-order structural phase transformation has been observed at 4.0 GPa in compression at room temperature, and at 3.6 GPa at 500 K. Thus, the transition pressure decreases with increasing temperature. In decompression, there is a hysteresis of 1.6 GPa at room temperature, and 0.9 GPa at 500 K.

The experimental zero-pressure bulk modulus of the tetragonal low-pressure phase is 64.7(7) GPa in good agreement with the theoretical value 66.3 GPa. The latter has been calculated using the tight-binding linear muffin-tin orbital method within the local density approximation.

Tentatively, the high-pressure phase above 4.0 GPa has an orthorhombic crystal structure with space group *Pmmn* (59). The relative volume change at the tetragonal to orthorhombic phase transition is $\Delta V/V = -5.5\%$. Amorphization is observed
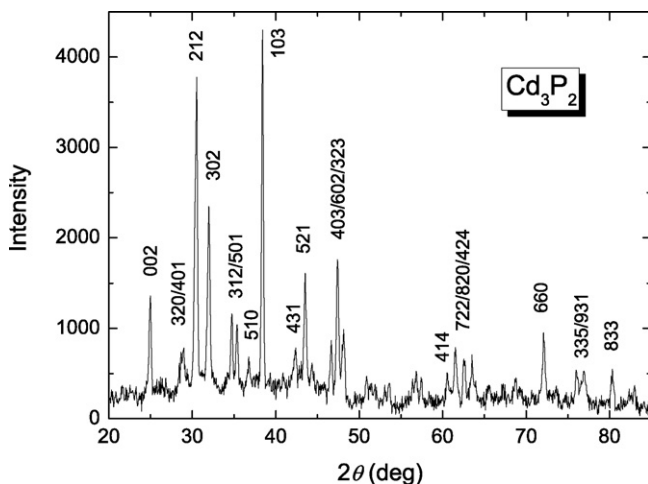
to occur at high pressure, and Cd_3P_2 is completely amorphous at 28 GPa.

A *P–T* phase diagram of Cd_3P_2 has been constructed on the basis of the electrical resistance measurements, thermo baric analysis and differential thermal analysis. A metastable phase of Cd_3P_2 has been observed in samples heated to above 600 K at about 3 GPa. A hexagonal unit cell can describe the crystal structure of the new phase.

Acknowledgements

References

[1] M.V. Stackelberg, R. Paulus, Z. Phys. Chem. B 28 (1935) 427.
[2] C.W.F.T. Pistorius, J.B. Clark, J.C. Coetzer, G.J. Kruger, O.A. Kunze, High Temp.-High Press. 9 (1977) 471.
[3] G. Haacke, G.A. Castellion, J. Appl. Phys. 35 (1964) 2484.
[4] W. Zdanowicz, A. Wojakowski, Phys. Status Solidi 8 (1965) 569.
[5] S.G. Bishop, W.J. Moore, E.M. Swiggard, Solid State Commun. 7 (1969) xi.
[6] S.G. Bishop, W.J. Moore, E.M. Swiggard, Appl. Phys. Lett. 15 (1969) 12.
[7] S.G. Bishop, W.J. Moore, E.M. Swiggard, Appl. Phys. Lett. 16 (1970) 459.
[8] V.V. Sobolev, N.N. Syrbu, Phys. Status Solidi (b) 64 (1974) 423.
[9] J. Cisowski, J. Pastuszka, K. Kloc, Acta Phys. Pol. A 58 (1980) 737.
[10] D.R. Rao, A. Nayak, J. Mater. Sci. 17 (1992) 4389.
[11] P.J. Lin-Chung, Phys. Status Solidi (b) 47 (1971) 33.
[12] P. Plenkiewicz, B. Dowgiallo-Plenkiewicz, Phys. Status Solidi (b) 92 (1979) 379.
[13] P. Plenkiewicz, B. Dowgiallo-Plenkiewicz, Phys. Status Solidi (b) 95 (1979) 29.
[14] A. Waśkowska, L. Gerward, J.S. Olsen, G. Vaitheeswaran, V. Kanchana, F.S. Yel'kin, V.A. Sidorov, Proceedings of the Joint 20th AIRAPT–43th EHPRG Conference, Karlsruhe, 2005.
[15] L.G. Khvostantsev, L.F. Vereshchagin, A.P. Novikov, High Temp.-High Press. 9 (1977) 637.
[16] L.G. Khvostantsev, V.N. Slesarev, V.V. Brazhkin, High Press. Res. 24 (2004) 371.
[17] L.G. Khvostantsev, V.A. Sidorov, O.B. Tsiok, in: M.H. Manghnani, T. Yagi (Eds.), Properties of Earth and Planetary Materials at High Pressure and Temperature, Geophysical Monograph 101, American Geophysical Union, Washington, DC, 1998, p. 89.
[18] J.S. Olsen, Rev. Sci. Instrum. 83 (1992) 1058.
[19] G. Huber, K. Syassen, W.B. Holzapfel, Phys. Rev. B 15 (1977) 5123.
[20] H.K. Mao, J. Xu, P.M. Bell, J. Geophys. Res. 91 (1986) 4673.
[21] P.-E. Werner, Ark. Kem. 31 (1969) 513.
[22] F.J. Birch, J. Appl. Phys. 9 (1938) 279.
[23] F.J. Birch, Phys. Rev. 71 (1947) 809.
[24] O.K. Andersen, Phys. Rev. B 12 (1975) 3060.
[25] U. von Barth, L. Hedin, J. Phys. C: Solid State Phys. 5 (1972) 1629.
[26] O.K. Andersen, O. Jepsen, Phys. Rev. Lett. 53 (1984) 2571.
[27] G. Krier, O. Jepsen, O.K. Andersen, unpublished data.
[28] C.W.F.T. Pistorius, High Temp.-High Press. 7 (1975) 441.
[29] K.A. Dobryden, Inorg. Mater. (Engl. Transl.) 9 (1972) 1372.
[30] V.I. Psarev, K.A. Dobryden, Inorg. Mater. (Engl. Transl.) 6 (1970) 203.
[31] E. Wu, PowdMult, An Interactive X-ray Powder Diffraction Data Interpretation and Indexing Program, Version 2.2, 1978.